Quarterly Reviews of Biophysics

www.cambridge.org/qrb

Using multiscale molecular dynamics simulations to explore the fusion machinery underlying neurotransmitter release

Dong An[1], Satyan Sharma[2] and Manfred Lindau[1]

[1]Department of Physiology and Biophysics, University of Miami Miller School, Miami, FL, USA and [2]Department of Chemistry – BMC, Uppsala University, Uppsala, Sweden

Review

Cite this article: An D, Sharma S and Lindau M (2025). Using multiscale molecular dynamics simulations to explore the fusion machinery underlying neurotransmitter release. *Quarterly Reviews of Biophysics*, **58**, e14, 1–14
https://doi.org/10.1017/S0033583525100048

Received: 09 May 2025
Revised: 13 June 2025
Accepted: 21 June 2025

Keywords:
fusion machinery; MD simulation; membrane fusion; neurotransmission; SNARE complex

Corresponding author:
Manfred Lindau;
Email: mxl2044@miami.edu

Abstract

Neurotransmitter release via synaptic vesicle fusion with the plasma membrane is driven by SNARE proteins (Synaptobrevin, Syntaxin, and SNAP-25) and accessory proteins (Synaptotagmin, Complexin, Munc13, and Munc18). While extensively studied experimentally, the precise mechanisms and dynamics remain elusive due to spatiotemporal limitations. Molecular dynamics (MD) simulations—both all-atom (AA) and coarse-grained (CG)—bridge these gaps by capturing fusion dynamics beyond experimental resolution. This review explores the use of these simulations in understanding SNARE-mediated membrane fusion and its regulation by Synaptotagmin and Complexin. We first examine two competing hypotheses regarding the driving force of fusion: (1) SNARE zippering transducing energy through rigid juxtamembrane domains (JMDs) and (2) SNAREs generating entropic forces via flexible JMDs. Despite different origins of forces, the conserved fusion pathway – from membrane adhesion to stalk and fusion pore (FP) formation – emerges across models. We also highlight the critical role of SNARE transmembrane domains (TMDs) and their regulation by post-translational modifications like palmitoylation in fast fusion. Further, we review Ca^{2+}-dependent interactions of Synaptotagmin's C2 domains with lipids and SNAREs at the primary and tripartite interfaces, and how these interactions regulate fusion timing. Complexin's role in clamping spontaneous fusion while facilitating evoked release via its central and accessory helices is also discussed. We present a case study leveraging AA and CG simulations to investigate ion selectivity in FPs, balancing timescale and accuracy. We conclude with the limitations in current simulations and using AI tools to construct complete fusion machinery and explore isoform-specific functions in fusion machinery.

Table of contents

Introduction

Neurons communicate by releasing neurotransmitters at the synapse, a process driven by the fusion of synaptic vesicles with the plasma membrane (Südhof, 2008). This fusion event, mediated by the fusion machinery, occurs within a submillisecond timescale following an action potential, triggering presynaptic Ca currents which activate fusion (Borst and Sakmann, 1998; Südhof, 2013). The transmitter that is released binds to postsynaptic receptors, triggering postsynaptic currents (Südhof, 2013). But what are the components of this machinery, and how do they work together to achieve such rapid fusion?

At the end of the 20th century, experiments identified the core of the fusion machinery as the SNARE complex, composed of Synaptobrevin 2 (Syb2), Syntaxin-1 (Stx1), and SNAP-25 (Baumert *et al.*, 1989; Oyler *et al.*, 1989; Bennett *et al.*, 1992; Sollner *et al.*, 1993), along with several accessory proteins, including Synaptotagmin (Syt), Complexin (Cpx), Munc13, and Munc18 (Perin *et al.*, 1990; Hata *et al.*, 1993; Brose *et al.*, 1995; McMahon *et al.*, 1995) (Figure 1*a*). in vitro reconstitution experiments demonstrated that Syb2, located on synaptic vesicles (Baumert *et al.*, 1989), and Stx1 and SNAP-25, on the plasma membrane (Oyler *et al.*, 1989; Bennett *et al.*, 1992), self-assemble into a SNARE complex (Fasshauer and Margittai, 2004). This complex forms the minimal machinery necessary for vesicle fusion (Weber *et al.*, 1998). Subsequent studies identified Syt as the calcium sensor that detects Ca^{2+} influx through voltage-gated calcium channels via its C2 domains, triggering Ca^{2+}-evoked release (Li *et al.*, 1995; Chapman, 2002) while clamping spontaneous fusion by maintaining vesicle priming (Voleti *et al.*, 2020; Rizo, 2022). Different Syt isoforms serve at different speeds of release upon Ca signals. The fast Ca sensor Syt1 mediates synchronous release, whereas the slow sensor Syt7 was reported to

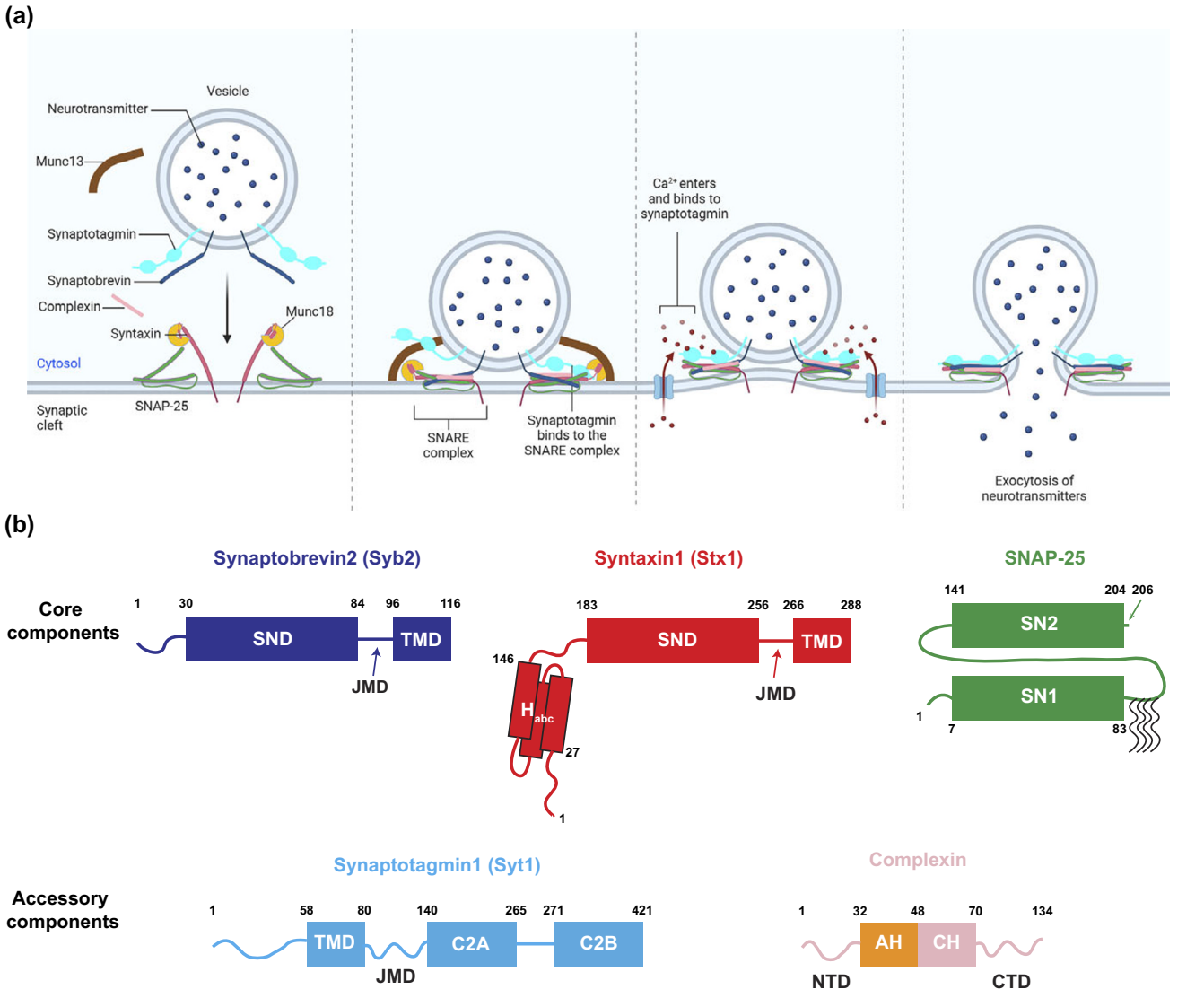

Figure 1. Components of the SNARE-mediated membrane fusion machinery.
(*a*) The fusion machinery is composed of core SNARE proteins – Syb2, Stx1, and SNAP-25 – along with accessory regulatory proteins such as Syt1, Cpx, Munc13, and Munc18. These components cooperate to rapidly drive neurotransmitter release. (*b*) Protein Domain Strucures. Syb2 and Stx1 each contain one SND and one TMD, connected by a JMD (Stein *et al.*, 2009). Unlike Syb2, which has only an unstructured N-terminal domain (NTD), Stx1 contains an N-terminal H_{abc} domain composed of three helices, connected to the SND via a 37-residue linker. SNAP-25 has two SNARE domains, SN1 and SN2, connected by a 58-residue linker, with several N-terminal residues (positions 85, 88, 90, and 92) that are commonly palmitoylated (Veit *et al.*, 1996). The Ca^{2+} sensor Syt1 is located on synaptic vesicles, with its TMD at the N-terminus. A 60-residue JMD connects the TMD to the C-terminal tandem C2 domains (C2A and C2B), which mediate Ca^{2+} binding (Fernandez *et al.*, 2001). Complexin contains several helical domains including the accessory helix (AH) and the central helix (CH), flanked by an NTD and a C-terminal domain (CTD), respectively (Rizo, 2022). All residues at the edge of domains are marked with residue numbers.

https://doi.org/10.1017/S0033583525100048

trigger asynchronous release (Bacaj *et al.*, 2013). Subsequently, Syt7 was found to function in Ca^{2+}-dependent synaptic vesicle replenishment in interaction with calmodulin (Liu *et al.*, 2014). Cpx was later recognized as a modulator of neurotransmitter release, both inhibiting spontaneous fusion and enhancing Ca^{2+}-evoked release (Jorquera *et al.*, 2012; Li *et al.*, 2024). Additionally, Munc13 and Munc18 facilitate SNARE complex assembly and vesicle docking and priming while competing with their disassembly by N-ethylmaleimide–sensitive factor (NSF) and one of the soluble NSF attachment proteins (α-SNAP) (Ma *et al.*, 2013; Liu *et al.*, 2016; White *et al.*, 2018; Rizo, 2022).

Despite extensive experimental studies elucidating the roles of SNARE proteins and their regulators, directly visualizing membrane fusion – how the fusion machinery assembles, reshapes membranes, and drives neurotransmitter release – remains a challenge due to the nanometer-scale dimensions (Jung, 2019) and transient kinetics of this process (Sabatini and Regehr, 1996; Acuna *et al.*, 2014). Molecular dynamics (MD) simulations have emerged as a powerful complementary approach, providing details of protein–protein and protein–lipid interactions that are otherwise inaccessible. These simulations not only generate dynamic 'movies' of membrane fusion but also offer mechanistic insights that can guide future experiments.

MD simulations offer a choice between different levels of resolution: all-atom (AA) simulations, which model every atom for high accuracy in molecular interactions and motions, and coarse-grained (CG) simulations, which simplify molecular representations to capture large-scale conformational changes over extended timescales (Marrink *et al.*, 2007; Deserno, 2009). These simulations provide a diversity of insight to uncover the mechanism of the fusion machinery to cooperatively and rapidly fuse membranes.

For CG simulations, we mainly discuss two kinds of force fields: The MARTINI force field (Marrink *et al.*, 2004, 2007; Monticelli *et al.*, 2008) and an ultra-coarse-grain (UCG) force field applied in the O'Shaughnessy group (Mostafavi *et al.*, 2017; McDargh *et al.*, 2018; Butu *et al.*, 2025). The MARTINI (https://cgmartini.nl/) force field represents a molecule based on a four-to-one mapping scheme (Marrink *et al.*, 2004, 2007; Monticelli *et al.*, 2008) (About four non-hydrogen atoms and associated hydrogens are represented by a single bead). Some chemical groups, like ring-like compounds, are represented with higher resolution with a bead representing two non-hydrogen atoms and associated hydrogens. Only five main types of interactions, namely polar, non-polar, apolar, charged, and halogen, are defined. The bonded interactions are typically derived from AA simulations, and the non-bonded interactions are tuned based on the reproduction of experimental free energies between polar and apolar phases of chemical compounds. Using the CG MARTINI force field accelerates molecular dynamics like diffusion by a factor of 4 (Marrink *et al.*, 2004, 2007). The UCG representations are much more coarse grained than the MARTINI force field (Mostafavi *et al.*, 2017; McDargh *et al.*, 2018; Butu *et al.*, 2025). For the SNARE proteins, one bead represents a group of four residues and representations of lipids, adopted from (Illya and Deserno (2008), use only four beads to represent a lipid molecule. The solvent molecules are represented implicitly. This UCG method significantly increases the dynamics such that the simulation can easily reach milliseconds.

In this review, we explore how multiscale MD simulations have advanced our understanding of SNARE-mediated membrane fusion. We begin by examining current perspectives on how SNARE complexes generate forces to remodel membranes – whether through SNARE domain (SND) zippering, entropic forces, or a combination of both – by analyzing the roles of SNARE juxtamembrane domains (JMDs) and transmembrane domains (TMDs) (Figure 1*b*). We then discuss possible pathways leading to fusion pore (FP) formation and the kinetics governing this process. Next, we highlight how MD simulations have provided insights into how Syt1 C2 domains regulate SNARE dynamics to achieve Ca^{2+} sensing, as well as the potential roles of Cpx in modulating fusion by either clamping or facilitating it under different conditions. We also examine the complementary use of AA and CG simulations, balancing accuracy and computational efficiency to capture both molecular interactions and long-timescale dynamics. Finally, we discuss how AI tools like AlphaFold and Robetta have expanded the scope of MD simulations by improving protein structure predictions, enabling the study of isoform-specific differences, and facilitating the integration of additional fusion machinery components into simulations.

SNARE complex: The core engine of membrane fusion

SNARE zippering and membrane contact formation

Since Weber et al. discovered that SNARE proteins form the minimal membrane fusion machinery (Weber *et al.*, 1998), a key question has been how SNARE proteins drive vesicle–plasma membrane fusion. SNARE complexes are formed by 1 R-SND and 3 Q-SNDs whose layer 0 residue at the center of their SNDs are Arginine (R) and Glutamine (Q), respectively (Yadav *et al.*, 2024). Experiments have shown that in the neuronal SNARE complex the R-SNARE Syb2 zippers into the Stx-SNAP25 t-SNARE (Q-SNARE) complex, forming a coiled coil structure (Chen *et al.*, 2001). The zippering is exergonic and for the amount of energy released during zippering estimates in the range of 30–85 kT have been reported (Wiederhold and Fasshauer, 2009; Gao *et al.*, 2012; Ma *et al.*, 2015; Zhang and Hughson, 2021; Jahn *et al.*, 2024). However, the roles of the SNDs, JMDs and TMDs in this process remain controversial. Two competing hypotheses for the origins of the SNARE complex driving forces to achieve fusion have emerged: (1) the released energy during SND zippering is transduced to the TMDs via rigid JMDs, bringing the two membranes into close proximity and enabling neurotransmission (Figure 2*a*) (Südhof and Rothman, 2009; Jackson, 2010; Zhang and Hughson, 2021), or (2) SNARE complexes bring the membranes together via entropic forces generated by thermodynamic fluctuations of the SNARE domains to enable a larger available space for SND occupancy, whereas the SND zippering energy had been dissipated, transduced by flexible JMDs (Figure 2*b*) (Mostafavi *et al.*, 2017; McDargh *et al.*, 2018; Butu *et al.*, 2025). For more detailed discussions of the pathways of SNARE assembly, fusion triggering, and disassembly see (Jahn *et al.*, 2024). In this section, we review and focus primarily on the evidence from MD simulations supporting these hypotheses.

The rigid JMD model aligns with the crystal structure of the post-fusion SNARE complex, which reveals a helical JMD (PDB: 3HD7) (Stein *et al.*, 2009). In 2011, Risselada et al. developed the first MARTINI-based membrane fusion system, in which two 20 nm vesicles were bridged by two SNARE complexes with structured and rigid JMDs (Risselada *et al.*, 2011). Upon SNARE zippering, the SNARE complexes brought the membranes into close proximity, leading to FP formation within microseconds. However, when the JMDs were modeled as unstructured and flexible, fusion was abolished on this timescale. Similar results were later obtained in a vesicle–planar membrane fusion system, further reinforcing the importance of JMD rigidity (Risselada and Grubmuller, 2012).

https://doi.org/10.1017/S0033583525100048

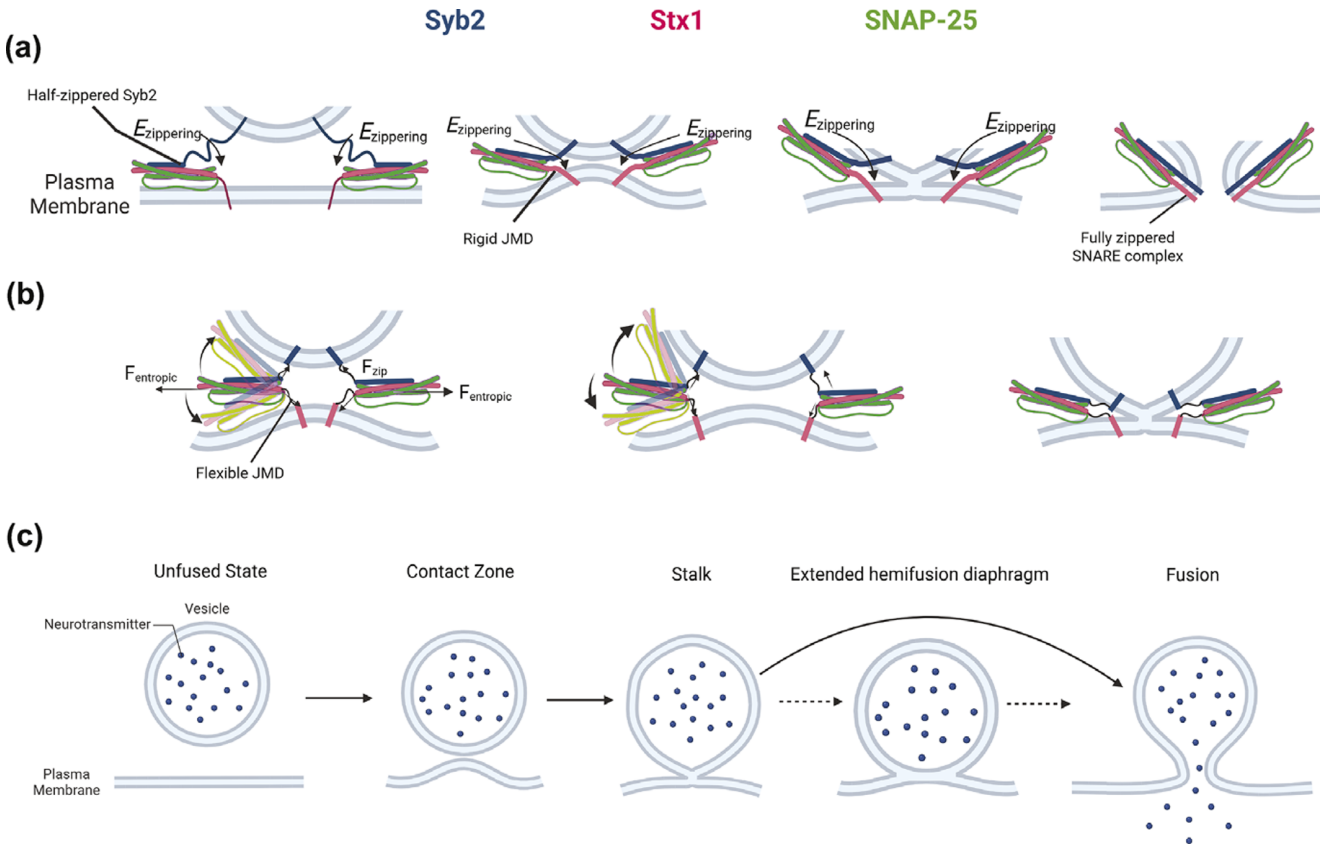

Figure 2. Contrasting hypotheses and shared features of how SNARE complexes drive membrane fusion.
(*a*) In the zippering-driven model, energy from SNARE complex zippering is transmitted via rigid and helical JMDs – represented by thick lines – which press the two membranes together, initiating stalk formation and subsequently FP opening. This process is facilitated by interactions between the C-terminal residues of Syb2 and Stx1 (Sharma and Lindau, 2018; An *et al.*, 2025). (*b*) In the entropic force model, thermal fluctuations of the SNDs generate entropic forces that expand the accessible conformational space for SND occupancy. In this case, zippering energy is dissipated, and flexible JMDs – represented by thin, curved lines – enable membrane contact, leading to reversible stalk formation and eventual FP opening (Butu *et al.*, 2025). (*c*) A generalized membrane fusion pathway shared by all MD simulations. The two membranes first adhere through a contact zone, followed by stalk formation via fusion of the cytoplasmic leaflet of the vesicle and the intracellular leaflet of the plasma membrane. The stalk then either expands into an extended HD – which can impede rapid fusion – or progresses to full fusion via FP formation.

This view is also supported by the CGMD simulations in ref. Fortoul *et al.* (2018) using a different force field.

Additional support for the rigid JMD hypothesis comes from simulations by Sharma and Lindau, who modeled fusion between a 40 nm vesicle and a planar plasma membrane bridged by six SNARE complexes (Sharma and Lindau, 2018). Here, rigid JMDs and constrained distances to the center of mass of the layer 0 backbone beads facilitated spontaneous fusion within microseconds (Figure 2*a*). Moreover, AA simulations initiated from SNARE complexes with unstructured JMDs have demonstrated that progressive structuring and zippering of the SNARE JMDs enables lipid tail interdigitation, ultimately accomplishing FP formation on a similar timescale (Rizo *et al.*, 2024).

However, this model has been challenged by findings that elongating the SNARE JMDs does not abolish fusion but instead slows down fusion kinetics (McNew *et al.*, 1999; Kesavan *et al.*, 2007). These findings led to the alternative hypothesis that SNARE-mediated fusion may primarily be driven by entropic forces rather than direct mechanical transduction (Mostafavi *et al.*, 2017; McDargh *et al.*, 2018; Butu *et al.*, 2025). To test this hypothesis, O'Shaughnessy's group developed an UCG model capable of reaching millisecond timescales. In their early models, SNARE complexes were represented as rod-like chains of beads for the SNARE domain, with unstructured JMDs modeled using a worm-like chain representation, while membranes were treated as rigid surfaces (Mostafavi *et al.*, 2017; McDargh *et al.*, 2018). In a more recent iteration, TMDs were explicitly included, and lipid representations were adapted from previous studies (Cooke *et al.*, 2005; Illya and Deserno, 2008) to allow direct visualization of membrane fusion rather than relying on inferred membrane-pressing energy (Butu *et al.*, 2025) (Figure 2*b*).

These simulations demonstrated that SNARE complexes could spontaneously generate ~8 pN of entropic force per complex, resulting in ~19 pN of membrane-pressing force per SNARE because of constant collisions and the trans-SNARE complex geometry which the vector of JMDs is bent ~67° away from that of SNARE domains in simulations. This force was sufficient to drive the formation of an extended fusion site, initiating membrane contact and ultimately leading to fusion (Butu *et al.*, 2025). Notably, these findings suggest that the presence of more SNARE complexes accelerates fusion kinetics.

Role of the JMD

The role of the SNARE JMD remains controversial, as evidence supporting both hypotheses has been reported. An early AA simulation study in 2003 found that increasing the concentration of the anionic lipid phosphatidylserine (PS) enhanced the helicity and rigidity of the Stx1A JMD (Knecht and Grubmuller, 2003). CG

https://doi.org/10.1017/S0033583525100048

simulations in MARTINI force field demonstrated that phosphatidylinositol 4,5-bisphosphate (PIP_2), a multivalent anionic lipid in the cytoplasmic leaflet of the plasma membrane, was enriched around the cationic Stx1A JMD (Sharma and Lindau, 2017). Taken together, these studies suggest that the PIP_2 enrichment at the Stx1A JMD could further stabilize its helical structure and potentially facilitate transduction of the 30–85 kT zippering energy via the helical JMDs to squeeze together and fuse the two membranes. However, it is still unknown how much energy is transduced to nucleate membrane fusion because it is not clear how specific structural features are connected to the fusion pathways, and the involved energies are model-dependent (Jahn *et al.*, 2024). Further, electron paramagnetic resonance (EPR) and nuclear magnetic resonance (NMR) experiments showed that the Stx1A JMD remained unstructured in vitro (Kim *et al.*, 2002; Lakomek *et al.*, 2019), challenging the notion that its helicity is a defining feature under all conditions. The structural characterization of these studies was, however, performed on isolated proteins and not on full SNARE complexes.

Pathway to fusion: From membrane contact to FP formation

A key question in membrane fusion research was whether the FP is proteinaceous or lipidic (Almers and Tse, 1990; Zimmerberg *et al.*, 1993; Lindau and Almers, 1995; Jackson, 2010). Before the discovery of SNARE proteins, membrane fusion pathways had been studied for ~50 years, beginning with in vitro experiments showing that membrane fusion was induced solely by Ca^{2+} (Ginsberg, 1978; Ohki, 1982; Ohki and Ohshima, 1985; Rand *et al.*, 1985; Kachar *et al.*, 1986; Nikolaus *et al.*, 2010). Also, the conductance of FP has been studied extensively (Breckenridge and Almers, 1987; Hartmann and Lindau, 1995; Lindau and Almers, 1995; Han *et al.*, 2004; Gong *et al.*, 2007). Based on experimental evidence, the widely accepted model of membrane fusion follows a sequential pathway involving: (1) membrane docking and priming, forming a potential fusion site (Fortoul *et al.*, 2015; Witkowska *et al.*, 2021; An and Lindau, 2024), (2) stalk nucleation (Sharma and Lindau, 2018), and (3) FP opening from the stalk state (Chernomordik and Kozlov, 2008; Kozlov *et al.*, 2010; Fang and Lindau, 2014; Jahn *et al.*, 2024) (Figure 2*c*). This pathway appears to be evolutionarily conserved, as extended hemifusion diaphragms (HDs) have been observed in both in vitro and in vivo studies but do not lead to rapid fusion (Figure 2*c*) (Diao *et al.*, 2012; Hernandez *et al.*, 2012; Zhao *et al.*, 2016).

MD simulations have consistently reproduced this pathway (Risselada *et al.*, 2011; Risselada and Grubmuller, 2012; Sharma and Lindau, 2018; Butu *et al.*, 2025). Initially, membrane adhesion and fusion site formation occur through either mechanical transduction of SNARE domain zippering or entropic forces. Subsequently, fusion proceeds via stalk nucleation, during which the TMD of Syb2 begins to approach that of Stx1. Finally, FP formation is facilitated by the hydrophilic C-terminal residues of Syb2 and Stx1. This pathway is also valid under membranes with asymmetric compositions (Sharma and Lindau, 2018) introduced from ref (Sharma *et al.*, 2015). Even though in some cases, additional intermediate structures, such as inverted micelles, have been occasionally observed (Risselada and Grubmuller, 2012; Sharma and Lindau, 2018), the overall membrane fusion pathway is similar among all MD simulations among different CG scales.

On the other hand, estimating the energy barriers between membrane docking, priming, stalk, hemifusion, and FP formation and the kinetics of the intermediate states based on MD simulations provides highly variable values among different force fields. Also, while extended HDs have been observed in multiple experimental studies (Nikolaus *et al.*, 2010; Diao *et al.*, 2012; Hernandez *et al.*, 2012; Zhao *et al.*, 2016), their roles in FP formation remain unclear. Instead of serving as an obligatory intermediate for rapid fusion, extended HDs may actually impair FP formation.

In CG simulations with MARTINI force field of a 40-nm vesicle fusing with a planar plasma membrane via six SNARE complexes – without constraints on the center-of-mass distances of layer 0 backbone beads – an extended HD formed, but no FP opened within 2 μs (Sharma and Lindau, 2018). This also aligns with in vivo experimental observations where extended HDs persisted for timescales ranging from 0.2 to 26 s in ~15% of fusion events, even exceeding experimental observation windows in ~30% of fusion events, whereas ~55% of the events showed fusion occurred immediately with no observation of extended HDs (Zhao *et al.*, 2016).

In contrast, MD simulations that exhibited rapid fusion – within microseconds for AA and CG simulations with MARTINI force field (Risselada *et al.*, 2011; Risselada and Grubmuller, 2012; Sharma and Lindau, 2018) and within milliseconds for UCG models (Butu *et al.*, 2025) – did not report the presence of extended HDs. This discrepancy may be explained by theoretical analysis suggesting that extended HDs drain membrane tension and stabilize the HDs, thereby preventing HD rupture and FP formation (Warner and O'Shaughnessy, 2012a, 2012b; Warner *et al.*, 2023).

SNARE TMDs in FP formation

As originally reported for fusion mediated by Influenza hemagglutinin (HA) lacking the TMD and anchored in membranes via a glycosylphosphatidylinositol (GPI) tail, the GPI-anchored HA mediated lipid mixing (hemifusion) but no full fusion (content mixing) (Kemble *et al.*, 1994). Correspondingly, it was found that lipid-anchored Syb2 failed to support fusion (Chang *et al.*, 2016). Several studies, including both experiments and MD simulations, indicate that TMDs play a crucial role in facilitating fast membrane fusion (reviewed in Fang and Lindau, 2014).

To investigate the function of the Syb2 TMD, Lindau et al. performed MARTINI MD simulations and found that ~70 kJ/mol of energy is required to extract Syb2 TMD from the synaptic vesicle (SV) membrane. This anchoring is stabilized by hydrophilic C-terminal residues as well as W89 and W90 (Lindau *et al.*, 2012). Beyond its anchoring role, the Syb2 TMD has been shown to actively contribute to FP dynamics. Combining in vivo experiments with AA simulations, Dhara et al. demonstrated that Syb2 TMD flexibility catalyzes both FP formation and expansion (Dhara *et al.*, 2016), and Han et al. showed that the flexibility of Syb2 TMD favors the helicity of JMD (Han *et al.*, 2016). Similarly, MARTINI MD simulations have revealed that Stx1A TMD lowers the free energy barrier for stalk formation, likely by inducing local membrane dimpling near the TMD insertion site on the plasma membrane (Smirnova *et al.*, 2019).

Beyond the intrinsic properties of TMDs, post-translational modifications such as palmitoylation also modulate SNARE function. in vivo experiments by Vardar et al. showed that palmitoylation of the Stx1A TMD enhances spontaneous neurotransmitter release but does not significantly alter Ca^{2+}-evoked release (Vardar *et al.*, 2022). To further investigate the effects of Stx1A TMD palmitoylation, we constructed a MARTINI MD model of palmitoylated Stx1A (residues 189–288). These simulations suggest that palmitoylation stabilizes a Stx1A TMD conformation, resembling its structure within the Stx1A–SNAP25 t-SNARE complex, potentially facilitating t-SNARE assembly (An *et al.*, 2025). However, FP

https://doi.org/10.1017/S0033583525100048

simulations revealed that Stx1A palmitoylation only disrupts interactions with Syb2 TMD, which may delay FP opening. Additionally, analysis of Stx1A palmitoyl chain tilt angles suggests that the palmitoyl chains exert mechanical constraints on the FP, reducing both peak conductance and conductance fluctuations (An *et al.*, 2025).

Syt: The calcium sensor in fusion machinery

Multiple Syt interaction modes with SNARE complex

Since the discovery of Syt as a Ca^{2+} sensor, the precise mechanism by which it interacts with the SNARE complex to trigger membrane fusion remains under debate. Over the past decade, studies have identified multiple potential interaction interfaces between Syt and SNAREs. The Brunger group identified two distinct interfaces: the primary interface (Zhou *et al.*, 2015) and the tripartite interface (Zhou *et al.*, 2017. Additionally, Brewer et al. reported a polybasic interface where Syt–SNARE interactions occur (Brewer *et al.*, 2015).

Although these interfaces have been proposed as sites for Ca^{2+}-dependent regulation, it remains unclear which interaction mode (or combination thereof) is responsible for Ca^{2+} sensing and fusion clamping and triggering. Here, we review recent evidence and examine Syt–SNARE interactions through multiscale MD simulations to provide insights into their functional roles.

Ca^{2+}-dependent lipid binding

One question about the Ca^{2+}-regulation of Syt is focused on how Ca^{2+} binding alters interactions between its C2 domains (Figure 1*b*) and lipid molecules. To investigate Syt Ca^{2+} binding, AA simulations produced Syt1 structures with two Ca^{2+} ions chelated at the binding pocket of each C2 domain (Bykhovskaia, 2015). The simulations revealed that Syt1 conformational flexibility drastically increased upon Ca^{2+} binding. The separation distance between the C2A and C2B domains increased, and interdomain rotations became more frequent. These changes in the Syt1 conformational state, help initiating the fusion process. More recent studies demonstrated that Ca^{2+}-bound C2 domains are enriched in anionic lipids such as PS and PIP_2 around the Ca^{2+}-binding loops (CBLs), leading to significant membrane penetration of these loops (Bykhovskaia, 2021). Similarly, Bender et al. combined AA simulations with mass spectrometry and confirmed these Ca^{2+}-dependent C2 domain–lipid interactions, along with anionic lipid preference interactions (Bender *et al.*, 2024). While C2A prefers an orientation more perpendicular to the membranes, C2B attaches parallel to the membrane. Courtney et al., combining experimental and AA simulation studies, revealed that Syt7 C2B shows stronger membrane penetration than Syt1 C2B (Courtney *et al.*, 2023). Mehta et al., combining CG simulations with MARTINI3 force field and experiments showed that the Syt1 lysine-rich JMD regulates Ca^{2+} binding via liquid–liquid phase separations (LLPS) (Mehta *et al.*, 2024). They proposed that these interactions play a key role in facilitating Ca^{2+}-evoked neurotransmitter release.

To mimic Ca^{2} binding in the MARTINI2 force field aimed at extending the simulation timescale, we introduced charge-flip mutations (D303K, D309K, D363K, D365K, and D371K) in the C2B domain of Syt1. These mutations introduce more charge than the two Ca^{2+} ions that are thought to bind C2B (Fernandez *et al.*, 2001) to exaggerate the effect of Ca^{2+} binding and since more than 2 Ca^{2+} ions may be accumulated in the presence of PIP2 (Schiavo *et al.*, 1996). Membrane self-assembly simulations using the method of (Sharma *et al.*, 2015), revealed the burial of CBLs into the membrane (Figure 3,

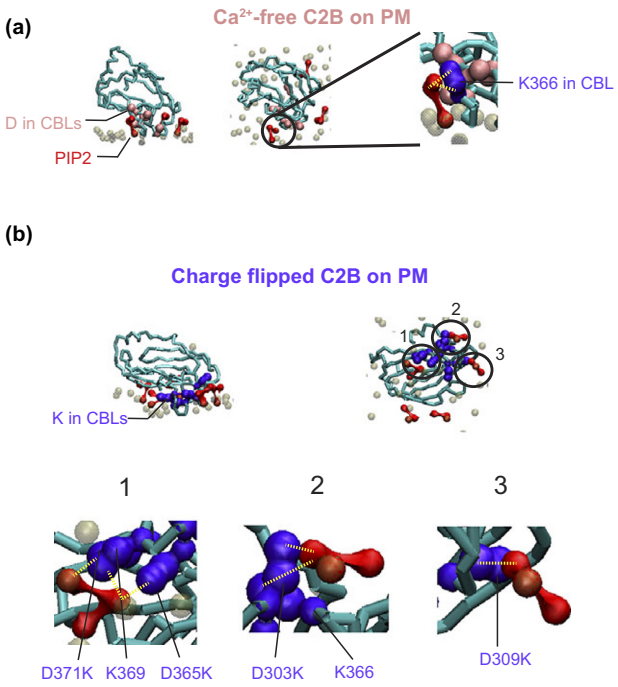

Figure 3. Charge-flip mutations in the C2B domain of Syt1 enhance interactions with PIP_2. Ca^{2+}-free (*a*) and charge-flip mutant (*b*) C2B domains of Syt1 (PDB: 5W5C (Zhou *et al.*, 2017)) inserted into a plasma membrane via self-assembly, using the protocol described in Sharma *et al.* (2015) with lipid composition from Sharma and Lindau (2018). Membranes were assembled in two stages: 50 ns simulations with x- and y-position restraints on the C2B domain, followed by 250 ns of unrestrained simulation. PIP_2 phosphate headgroup beads (PO4, P1 and P2) are colored red and the PO4 headgroup of the other phospholipids are colored brown transparently. The backbone of the C2B domains of Syt1 are colored in cyan. (*a*) Ca^{2+}-free C2B domain: The left and middle panels show side and top views at 9 ns of unrestrained simulation, highlighting interactions between the calcium binding loops (CBLs) of the Ca^{2+}-free C2B domain and PIP_2 headgroups. Anionic residues D303, D309, D363, D365, and D371 are shown in pink. Only one PIP_2 molecule interacts with the C2B domain in the circled region. The right panel zooms into this interaction, showing that the two phosphate groups on the inositol ring form a contact (~0.5 nm) with the sidechain of K366. (*b*) Charge-flip C2B mutant: The top panels show side and bottom views at 9 ns of unrestrained simulation for the charge-flip quintuple mutant D303K, D309K, D363K, D365K, and D371K (K; shown in purple). Three PIP_2 molecules are observed contacting the CBLs in the circled regions, driven by PIP_2–lysine interactions. The bottom row shows zoomed-in views of the three interaction regions. Region 1 shows one PIP_2 interacting with three lysine residues; region 2 with two lysines; and region 3 with one lysine – all at ~0.5 nm contact distance. The interacted lysines are annotated. This PIP_2 enrichment driven by the charge-flip mutant is consistent with prior all-atom simulations (Bykhovskaia, 2021; Bender *et al.*, 2024).

unpublished results). These CG simulations with MARTINI force field successfully reproduced Ca^{2+}-dependent PIP_2 enrichment in real plasma membrane composition, aligning with previous experimental and computational findings (Bykhovskaia, 2021; Bender *et al.*, 2024).

Ca^{2+}-dependent effect on SNARE-mediated fusion

A key question in the study of Syt is how Ca^{2+}-dependent lipid binding could alter SNARE conformation and dynamics to regulate FP formation. The primary interface has been proposed as the main site for transducing this effect, as its formation is independent of crystallization conditions (Zhou *et al.*, 2015, 2017), and its stability has been confirmed by AA simulations (Brunger and Leitz, 2023).

Using a combination of AA simulations and NMR studies, the Rizo/Rosenmund groups identified Syt1 C2B domain interactions

https://doi.org/10.1017/S0033583525100048

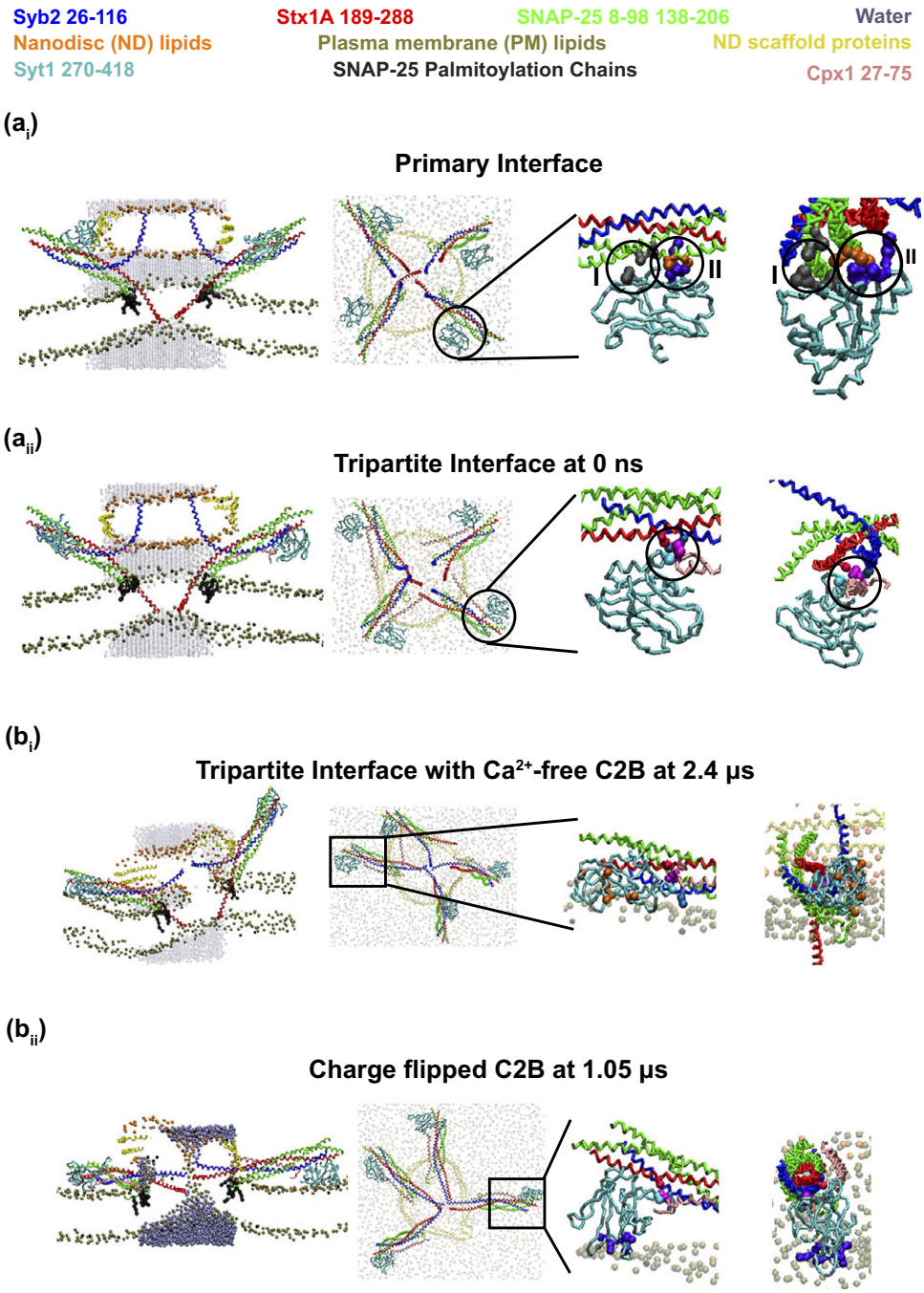

Figure 4. Regulation of Syt and Cpx in Neurotransmitter Release.
Syb2, Stx1A, SNAP-25, Syt1 C2B, and Cpx1 are colored blue, red, green, cyan, and pink, respectively. Water beads appear as transparent dark cyan, with one opaque bead marking an open FP. Lipid headgroups from the ND and plasma membrane are shown in orange and brown; the ND scaffold protein is yellow. SNAP-25 palmitoyl chains (black) are visible only in side views. (*a*) Initial configurations for FP simulations. Syt1 C2B domains were placed at the primary interface (a_i) or tripartite interface with Cpx1 (a_{ii}), by aligning crystal structure PDB 5W5C to the CG SNARE complex model (Sharma and Lindau, 2018) using PyMOL (DeLano, 2002). Side and top views are shown, with transparent membranes and ND. Zoomed-in panels (right) display interface details from views perpendicular or parallel to the SNARE axis. Primary interface (a_i): SNAP-25 interacts with C2B via Region I (SNAP-25: D166, E170; C2B: E295, Y338 colored in gray) and Region II (SNAP-25: D51, E52, E55 colored in orange; C2B: R281, R398, R399 colored in purple) circled in the two right panels. Tripartite interface (a_{ii}): Syb2, Stx1A, C2B domain of Syt1 and Cpx1 interact together (Syb2: R47 (blue); Stx1A: E211 (red); C2B: T383 (cyan); Cpx1: Y70 (light purple)) at the circle region. (b) Ca^{2+}-dependent effects on FP formation. (b_i) With Ca^{2+}-free C2B, 5/10 simulations stalled at hemifusion. At 2.40 μs, side/top views show incomplete SNARE zippering and Cpx1 AH crossing neighboring SNAREs as in Kümmel *et al.* (2011). Zoomed-in views show that CBLs remain unburied due to repulsive D residues (orange), though interprotein contacts shown above persist. (b_{ii}) With charge-flip C2B, all 10 simulations formed FPs (mean lag: 779 ± 176 ns). At 1.05 μs, SNAREs are fully zippered, and an FP is visible. The Cpx1 AH aligns parallel to Syb2, and charge-flipped CBLs contact the PO_4 plane, consistent with Ca^{2+}-triggered fusion. The Ca^{2+}-dependent states of SNARE–Syt–Cpx complexes are consistent with Figure 6B of Kümmel *et al.* (2011).

with SNAP-25 at two distinct regions within the SNARE complex: region I (including E295 and Y338) and region II (comprising R281, R398, and R399) (Figure 4a_i) (Toulmé *et al.*, 2024; Jaczynska *et al.*, 2025). Mutating E295 to alanine (E295A) enhanced the interactions at region I, leading to suppression of both Ca^{2+}-evoked and spontaneous release, while interactions at region II remained

https://doi.org/10.1017/S0033583525100048

intact (Toulmé *et al.*, 2024). Based on these findings, they proposed that C2B Ca^{2+} binding selectively modulates region I interactions, but not region II, to regulate Ca^{2+}-triggered membrane fusion. Recent AA simulations by Rizo et al. found that Syt1 C2 domains hinder SNARE-mediated fusion if placed close to the fusion site and suggested that binding of Syt1 at the primary interface keeps it away from the fusion site such that it does not interfere with FP formation (Rizo *et al.*, 2025). These studies led to the conclusion that Syt1 Ca^{2+} binding does not facilitate fusion by bridging membranes, inducing curvature, or perturbing membranes. They instead support the view Syt1 clamps fusion, being in the way at the fusion site and that Ca^{2+} binding may allow for its dissociation, enabling SNARE complex zippering. MARTINI (Sharma and Lindau, 2018) as well as AA simulations (Rizo *et al.*, 2024) have shown that in the absence of Syt, SNARE complex JMD linker zippering perturbs the bilayers, leading to FP formation.

Further doubts regarding the primary interface arose also from recent AA simulations, which suggested that Syt1 binding at this site forms a dead-end state, wherein Syt1 remains tightly attached to the plasma membrane but fails to insert into it upon Ca^{2+} binding (Bykhovskaia, 2024). Our own preliminary MARTINI FP simulations, in which a 10-nm nanodisc (ND) and a plasma membrane were bridged by four SNARE complexes unzipped up to layer 5 with C2B domains bound at each of the primary interfaces (Figure 4a_i, unpublished results), showed no significant change in the lag time preceding the first appearance of an FP conductance when the Ca^{2+}-bound mimic charge-flip mutations mentioned above were used (1452 ± 473 ns from 5 out of 10 simulations opened an FP within 4 μs for normal C2B versus 1512 ± 209 ns from 5 out of 10 simulations opened an FP within 4 μs for charge-flipped C2B, $p = 0.917$ in Kruskal test). The lag times were drastically increased compared to FP simulation without C2B bound at the primary interface (276 ± 20 ns from 10 out of 10 simulations opened an FP within 4 μs without C2B in ref. (An *et al.*, 2025)). Moreover, the primary interface does not include Syt–Cpx interactions, which have been implicated in Ca^{2+}-triggered fusion modulation (Bykhovskaia, 2024).

In contrast, our simulations suggest that Syt-SNARE binding at the tripartite interface, which includes Syt–Cpx interactions, facilitates FP opening in response to Ca^{2+} sensing – especially in the presence of the accessory helix (AH) of Cpx (Figure 4a_{ii}, *b*, unpublished results). This aligns with experimental findings showing that tripartite interface interactions are highly dynamic (Jaczynska *et al.*, 2023), increasing the likelihood that Ca^{2+}-dependent C2 domain–lipid interactions may disrupt Syt1–SNARE interactions to enable fusion.

Cpx: The fusion clamp and facilitator

Dual role of complexin in spontaneous and Ca^{2+}-evoked fusion

Cpx plays a paradoxical role in membrane fusion. Experimental evidence suggests that its N-terminal domain (NTD) acts as a catalyst for Ca^{2+}-evoked fusion, while its C-terminal domain (CTD) functions as an inhibitor of spontaneous fusion (Figure 1*b*) (Martin *et al.*, 2011; Jorquera *et al.*, 2012; Li *et al.*, 2024).

Despite this functional dichotomy, crystal structures reveal that the central helix (CH) of Cpx forms stable interactions with the groove between Syb2 and Stx1A within the SNARE complex (Bracher *et al.*, 2002; Chen *et al.*, 2002; Kümmel *et al.*, 2011), even in the presence of the Syt1 C2B domain at the tripartite interface (Zhou *et al.*, 2017. This raises a fundamental question: How does Syt1 regulate SNARE complex conformation and dynamics in a Ca^{2+}-dependent manner? To address this question, we review recent MD simulations of SNARE-mediated fusion that incorporate both the AH and CH of Cpx, shedding light on its regulatory mechanisms in SNARE-mediated fusion.

MD insights into Cpx inhibitory function

MD simulations of Cpx–SNARE interactions began in 2010 with Ghahremanpour et al., who investigated the role of the CH and AH of Cpx in SNARE complex interactions (Ghahremanpour *et al.*, 2010). Their AA simulations revealed: (1) The CH forms salt bridges and hydrogen bonds with the SNARE complex. (2) Cpx can also bind the t-SNARE complex (Stx1A and SNAP-25) in the absence of Syb2, reducing t-SNARE flexibility. (3) The AH and the C-terminal region of Syb2's SNARE domain interact with Stx1A, stabilizing the complex. However, AH proximity to Syb2 destabilizes Stx1A and the SN1 helix of SNAP-25, suggesting that Cpx inhibits membrane fusion by competing with Syb2 for t-SNARE binding.

In 2013, Bykhovskaia et al. combined AA simulations and in vivo experiments, confirming that Cpx interacts with Syb2 and SNAP-25 via salt bridges (Bykhovskaia *et al.*, 2013). These interactions stabilize SNARE complex unzippering up to layer 7, modulating the fusion process. Further studies demonstrated that Cpx–Syb2 interactions increase Cpx flexibility, preventing Syb2 from fully zippering and thereby clamping spontaneous fusion (Vasin *et al.*, 2016; Brady *et al.*, 2021).

Recently, Rizo et al. conducted AA simulations incorporating both the AH and CH of Cpx1 into a system containing a 20 nm vesicle and a planar membrane bridged by four SNARE complexes (Rizo *et al.*, 2022). Their findings showed that: (1) CH–SNARE interactions (via Y70) remained stable throughout the entire simulation. (2) The AH primarily interacted with the synaptic vesicle, likely exerting a steric effect that prevents membrane contact and fusion initiation. However, this steric hindrance may require longer simulation timescales to be fully explored.

Effects of Syt1 on Cpx-mediated SNARE regulation

Syt1 interacts with SNARE complexes not only at the primary interface but also at the tripartite interface, which is less stable and also involves Cpx (Zhou *et al.*, 2017). Given the complementary roles of Syt and Cpx, this interface is a potential candidate to regulate the transition enabling FP formation. We therefore performed preliminary MARTINI FP simulations of the tripartite interface incorporating Syt1, AH, and CH of Cpx1 in addition to the SNARE complexes. We found that the FP formation dynamics mediated by SNARE complexes was highly dependent on whether charge-flip mutations were applied to the C2B domain of Syt1: (1) In simulations with wild-type C2B, only 5 out of 10 trials resulted in FP formation within 4 μs. The mean lag time was 1278 ± 270 ns calculated from these five simulations. (2) In contrast, in simulations with charge-flipped C2B, 10 out of 10 trials resulted in FP formation, and the lag time was 779 ± 176 ns, even if $p = 0.066$.

Additionally, in wild-type C2B simulations, the AH of Cpx frequently interacted with the cytoplasmic leaflet of the ND and the intracellular leaflet of the plasma membrane during the stalk state, preventing full SNARE zippering (Figure 4b_i, unpublished results). SNARE complex zippering was occasionally obstructed by the AH attached to the neighbour SNARE complex. However, with charge-flipped C2B, SNARE complexes adopted orientations that facilitated the AH of Cpx staying parallel to the zippered SNARE complex, thereby enabling full zippering and FP opening (Figure 4b_{ii},

https://doi.org/10.1017/S0033583525100048

unpublished results). These observations seem consistent with the proposal that FP opening is enabled when the zippering obstruction by Cpx AH is removed (Kümmel *et al.*, 2011). Furthermore, combining AA simulations with in vitro experiments, Courtney et al., discovered that the Cpx C-terminal amphipathic helix stabilizes the FP via membrane interactions (Courtney *et al.*, 2022).

Back-mapping CG simulations to AA models: A case study on FP conductance

CG molecular representations are widely applied in MD to extend simulation timescales by reducing the atomic details of molecular systems. In some ultra-coarse-grained models, solvent molecules are represented implicitly, allowing simulations to reach millisecond timescales. However, this simplification comes at the cost of reduced accuracy in molecular interactions due to the loss of atomic resolution.

To overcome this limitation back-mapping of CG simulations to AA models has emerged as a powerful approach. CG simulations are employed to explore long-timescale phenomena and sample conformational space efficiently and then use back-mapping to refine the results and obtain high-resolution insights into specific interactions or structural features. This strategy allows for a more comprehensive understanding of complex biological processes, balancing the need for computational efficiency with the desire for atomic-level accuracy. Here, we review studies integrating MARTINI coarse-grained and AA force fields alongside experiments to uncover the molecular determinants of FP conductance (Sharma and Lindau, 2018; Delacruz *et al.*, 2021).

In these studies, the FP configuration was initially generated using CG simulations with MARTINI force field, as the computational simulation time required for FP opening is extremely long for direct AA simulations. The MARTINI force field represents four non-hydrogen atoms as a single coarse-grained bead, and groups four water molecules into a single water bead. This reduces thermal fluctuations, smooths the potential energy surface, and allows for longer simulation time steps, making millisecond-scale simulations feasible.

While CG simulations with MARTINI force field effectively capture bulk properties of proteins, membranes, and water, they can underestimate molecular interactions in nanometer-sized constricted pores, affecting the quantification of water and ion diffusivities. To address this, the system was back-mapped to an atomistic representation to recover finer molecular details. Back-mapping revealed a critical conductance threshold (~300 pS), below which ion selectivity emerged: cationic neurotransmitters (e.g., dopamine) were preferentially selected and permeable, whereas anionic neurotransmitters (e.g., glutamate) were blocked due to the anionic microenvironment within the narrow FP (Delacruz *et al.*, 2021). These findings highlight the necessity of back-mapping to accurately capture molecular interactions that govern neurotransmitter permeation and synaptic signaling. In addition, complementarity between AA and CG simulations was used to parametrize CG models and quantify the SNARE complex dynamics including the change of protein secondary structures (Darre *et al.*, 2012; Zheng, 2014).

Limitations and perspective

Limitations of current simulations

MD simulations are powerful tools for studying membrane fusion, but they are inherently limited by factors such as force field accuracy, system size, simulation timescale, and incomplete structural knowledge of proteins and complexes.

First, limitations in force fields – particularly in CG models – alongside constraints in system size and accessible timescales, cannot be simultaneously resolved without substantially increased computational resources. To simulate larger systems over longer timescales without increasing computational demand, more coarse-grained force fields must be used, at the cost of reduced chemical interaction resolution. As a result, dynamic properties like lipid diffusion are accelerated in CG models (Marrink *et al.*, 2004; Ingolfsson *et al.*, 2017). Furthermore, compromising chemical interaction resolution by CG can alter the energy landscape of interactions among components of the fusion machinery and that of interactions between the protein fusion machinery and lipids. The energy barriers of protein dynamics and membrane remodeling ultimately affect the kinetics of FP formation.

System size limitations can also introduce artifacts. When the natural diffusive distance of molecules exceeds the simulation box dimensions, periodic boundary conditions may induce non-physical dynamics or artificial interactions. To fit within these limitations, artificial geometries – such as 20 nm vesicles or 10 nm NDs – are often used instead of physiologically relevant 50 nm synaptic vesicles, which may compromise biological realism.

Likewise, timescale limitations pose a major challenge. Physiological fusion occurs on submillisecond timescales, which are difficult to reach, even with CG simulations. To observe fusion events within accessible timescales, researchers often introduce dynamics-accelerating factors, such as fusogenic lipid compositions or pre-constrained SNARE complex structures, based on the selected force field.

Beyond these intrinsic limitations, external limitations also exist – most notably, the lack of precise structural information for several key components of the fusion machinery. Although in vitro structures of post-fusion SNARE complexes and SNARE–Syt–Cpx assemblies have been resolved and are often used to derive initial conditions for simulations, the native, dynamic assemblies that govern membrane docking, priming, and fusion remain elusive due to their inherent structural flexibility and transient nature.

For example, Munc13 and Munc18 remain difficult to incorporate into simulations because their interaction interfaces with the SNARE complex and membranes are still unresolved. As a result, it is unclear how synaptic vesicles dock to the plasma membrane and how Syb2, Stx1, SNAP-25, Syt, and Cpx assemble into functional pre-fusion complexes with assistance from Munc13 and Munc18. Without knowledge of these 3D pre-fusion structures or the molecular architecture of vesicle docking sites, the physiologically accurate initial conditions for simulating neurotransmitter release remain uncertain. This in turn obscures our understanding of the temporal distribution of vesicle docking, priming, and fusion events during exocytosis.

To address this gap, Li et al used cryo-electron tomography to observe a symmetrical arrangement of six core components – likely including SNAREs, Syt, Cpx, and Munc13 – at the fusion site in nerve growth factor-differentiated neuroendocrine PC12 cells (Li *et al.*, 2019). Similar structural features were later observed in mouse hippocampal neurons (Radhakrishnan *et al.*, 2021). Building on this, the Rothman group proposed – based on reconstitution experiments in (Bera *et al.*, 2023) – that 12 SNARE complexes may assemble in a two-step process, coordinated by associated proteins such as Syt, Cpx, Munc13, and synaptophysin, forming a highly symmetric, ring-like structure (Rothman *et al.*, 2023). However, the detailed 3D structures of these assemblies are yet to be resolved.

https://doi.org/10.1017/S0033583525100048

Because of these challenges, using accurate protein complexes in fusion simulations is essential for generating realistic, dynamic representations of membrane fusion. Computational resources that reliably predict protein folding and protein–protein interactions are critical for addressing the current uncertainties surrounding physiological initial conditions.

In the following subsection, we briefly discuss structure prediction tools such as AlphaFold (https://deepmind.google/science/alphafold/), Robetta (https://robetta.bakerlab.org/), and SWISS-MODEL (https://swissmodel.expasy.org), which are capable of predicting the 3D structures of individual proteins and protein complexes. These tools are particularly valuable in reconstructing unknown assemblies involved in membrane fusion – especially following the development of AlphaFold2, which has significantly improved the accuracy of structure predictions (Bertoline *et al.*, 2023).

Completing protein structures and assembling complex systems

Filling the gaps between protein sequences and their corresponding 3D structures has been extensively studied for ~30 years. M. C. Peitsch established the first free server called SWISS-MODEL (Peitsch, 1996) to predict the protein 3D structures based on the homologous protein structures (Waterhouse *et al.*, 2018). This method is called Homology, which stems from the observation that the interacting interfaces among homologous complexes are often conserved (Zhang *et al.*, 2010), with the availability of conserved protein–protein interaction templates (Kundrotas *et al.*, 2012). In 2018, SWISS-MODEL was able to model both homomeric and heteromeric complexes (Waterhouse *et al.*, 2018). Another server called Robetta was established in Baker's lab applying Rosetta-based algorithms for *de novo* structure prediction (Rohl *et al.*, 2004). In the Rosetta method, short protein fragments are assembled in Monte Carlo strategy to generate native-like 3D conformations. This method yields very accurate predictions (0.3–0.6 nm alpha-carbon RMSD) compared to the experimental structures for proteins with 60 or more residues.

In the 2020s, with the increasing number of experimental solved structures (~ 240 k PDB structures archived in https://www.rcsb.org/) and the maturation of deep learning models, AI has been introduced into predicting protein 3D structures based on their amino acid sequences. According to the 14th Critical Assessment of Structure Prediction (CASP14) conference (https://predictioncenter.org/casp14/zscores_final.cgi), Alphafold2 and Robetta (using RoseTTAFold network) servers are the top2 most accurate models to predict protein 3D structures (Baek *et al.*, 2021; Bryant *et al.*, 2022) and have been awarded the Nobel prize in Chemistry in 2024 (Callaway, 2024). In addition, ColabFold is derived from Alphafold2 by improving the sequence search, providing powerful tools for modeling homomer and heteromer complexes (Mirdita *et al.*, 2022). ColabFold also exposes advanced functionality, expands the environmental databases, and enables large protein structure prediction scale, at about a 90-fold speed-up over AlphaFold2. Furthermore, Harmalkar et al., developed the improved version of ReplicaDock called AlphaRED (AlphaFold-initiated Replica Exchange Docking) by combining AlphaFold as a structural template generator to accurately predict protein–protein docking (Harmalkar *et al.*, 2025). Thus, AI models like AlphaFold (Jumper *et al.*, 2021), Colabfold (Mirdita *et al.*, 2022) and Robetta (Baek *et al.*, 2021) can help to address some of these external limitations by providing structural predictions for components of the fusion machinery. For more details, please see the minireview of Bertoline *et al.* (2023).

This advancement is particularly valuable for studying synaptic fusion machinery, as it allows for the modeling of full-length SNARE proteins and accessory factors such as Syt, Cpx, Munc13, and Munc18 to further approach a realistic structure of the fusion machine mediating transmitter release.

For instance, by aligning AlphaFold-predicted structures of Syb2, Stx1A, and SNAP-25 with crystal structures of the SNARE complex (PDB: 3HD7) (Stein *et al.*, 2009), a near-complete model of the synaptic vesicle fusion system can be assembled (An and Lindau, 2024). Similarly, tripartite interfaces involving Syt and Cpx can be reconstructed by integrating AlphaFold-predicted structures with known crystal structures of their interactions (PDB: 5W5C) (Zhou *et al.*, 2017).

Exploring isoform-specific differences

Beyond completing incomplete protein structures, AI models also facilitate the modeling of isoform-specific variations, offering insights into functional differences between isoforms. By aligning AlphaFold-predicted isoform structures and replacing the canonical protein with its isoform in MD simulations, it has been possible to investigate how sequence variations strengthen or weaken key interactions, ultimately influencing synaptic vesicle fusion.

For example, increased fusogenicity altering the size of the primed vesicle pool and the clamping of spontaneous neurotransmitter release of Stx2 compared to Stx1A has been attributed to sequence differences in the C-terminal Stx SNDs (Lázaro *et al.*, 2024). MD simulations could provide molecular insights into such Stx isoform differences, explaining why Stx2 SNARE complexes are more fusogenic than Stx1A SNARE complexes.

Similarly, MD simulations could be used to explore isoform-specific differences in accessory proteins. For example: (1) Syt1 versus Syt7, elucidating their distinct roles in fusion and docking for synchronous versus asynchronous release (Vevea *et al.*, 2021; Wu *et al.*, 2024), and how different membrane penetrations (Courtney *et al.*, 2023) alter SNARE–Syt interactions to fine-tune FP kinetics and (2) Cpx1 versus Cpx2, illustrating different roles of Cpxs in neurotransmission like Cpx2 rather than Cpx1 facilitates large dense core vesicle docking and priming in chromaffin cell exocytosis (Cai *et al.*, 2008).

Integrating AlphaFold-predicted structures with MD simulations offers great promise to bridge structural and functional gaps, and lead to a more comprehensive understanding of how protein isoforms modulate neurotransmitter release dynamics. This approach could also further provide guidance on future in vitro and in vivo experiments like mutating key residues to observe phenotypes to deeply understand the mechanisms of neurotransmission and the related diseases due to neurotransmitter release dysfunctions.

Declaration of generative AI and AI-assisted technologies in the writing process. During the preparation of this study the first author Dong An used ChatGPT in order to improve language and readability. After using this tool/service, the author(s) reviewed and edited the content as needed and took full responsibility for the content of the publication.

Acknowledgements. We thank Reinhard Jahn and Michael Kozlov for their critical reading of the manuscript and excellent comments and suggestions. Unpublished simulations were performed on Triton cluster from Frost Institute for Data Science and Computing (https://idsc.miami.edu/) and Bridges-2 at Pittsburgh Supercomputing Center through allocation BIO250019 and BIO250054 from the Advanced Cyberinfrastructure Coordination Ecosystem: Services & Support (ACCESS) program, which is supported by National Science Foundation grants #2138259, #2138286, #2138307, #2137603, and #2138296. Figures 1*a* and 2 were created with BioRender.com.

https://doi.org/10.1017/S0033583525100048

Financial support. This study has been supported by US National Institutes of Health (NIH) grant R35GM139608.

Competing interests. The authors declare none.

References

Acuna C *et al.* (2014) Microsecond dissection of neurotransmitter release: SNARE-complex assembly dictates speed and Ca sensitivity. *Neuron* **82**(5), 1088–1100. https://doi.org/10.1016/j.neuron.2014.04.020.

Almers W and Tse F (1990) Transmitter release from synapses: Does a preassembled fusion pore initiate exocytosis? *Neuron* **4**(6), 813–818.

An D *et al.* (2025) Syntaxin 1A Transmembrane domain Palmitoylation induces a Fusogenic conformation. *Biophysical Journal* **124**. https://doi.org/10.1016/j.bpj.2025.05.022.

An D and Lindau M (2024) Exploring the structural dynamics of the vesicle priming machinery. *Biochemical Society Transactions* **52**(4), 1715–1725. https://doi.org/10.1042/BST20231333.

Bacaj T *et al.* (2013) Synaptotagmin-1 and Synaptotagmin-7 trigger synchronous and asynchronous phases of neurotransmitter release. *Neuron* **80**(4), 947–959. https://doi.org/10.1016/j.neuron.2013.10.026.

Baek M, DiMaio F, Anishchenko I, Dauparas J, Ovchinnikov S, Lee GR, Wang J, Cong Q, Kinch LN, Schaeffer RD, Millán C, Park H, Adams C, Glassman CR, DeGiovanni A, Pereira JH, Rodrigues AV, van Dijk AA, Ebrecht AC, Opperman DJ, Sagmeister T, Buhlheller C, Pavkov-Keller T, Rathinaswamy MK, Dalwadi U, Yip CK, Burke JE, Garcia KC, Grishin NV, Adams PD, Read RJ and Baker D (2021) Accurate prediction of protein structures and interactions using a three-track neural network. *Science* **373**(6557), 871–+. https://doi.org/10.1126/science.abj8754.

Baumert M *et al.* (1989) Synaptobrevin: An integral membrane protein of 18,000 daltons present in small synaptic vesicles of rat brain. *The EMBO Journal* **8**(2), 379–384. https://doi.org/10.1002/j.1460-2075.1989.tb03388.x.

Bender J *et al.* (2024) Ca2+−dependent lipid preferences shape synaptotagmin-1 C2A and C2B dynamics: Insights from experiments and simulations. *Structure* **32**(10), 1691, e1695–1704.

Bennett MK *et al.* (1992) Syntaxin: A synaptic protein implicated in docking of synaptic vesicles at presynaptic active zones. *Science* **257**(5067), 255–259. https://doi.org/10.1126/science.1321498.

Bera M *et al.* (2023) Synaptophysin chaperones the assembly of 12 SNAREpins under each ready-release vesicle. *Proceedings of the National Academy of Sciences of the United States of America* **120**(45). https://doi.org/10.1073/pnas.2311484120.

Bertoline LMF *et al.* (2023) Before and after AlphaFold2: An overview of protein structure prediction. *Frontiers in Bioinformatics* **3**. https://doi.org/10.3389/fbinf.2023.1120370.

Borst JGG and Sakmann B (1998) Calcium current during a single action potential in a large presynaptic terminal of the rat brainstem. *Journal of Physiology-London* **506**(1), 143–157. https://doi.org/10.1111/j.1469-7793.1998.143bx.x.

Bracher A *et al.* (2002) X-ray structure of a neuronal complexin-SNARE complex from squid. *Journal of Biological Chemistry* **277**(29), 26517–26523. https://doi.org/10.1074/jbc.M203460200.

Brady J *et al.* (2021) The accessory helix of complexin stabilizes a partially unzippered state of the SNARE complex and mediates the complexin clamping function in vivo. *eNeuro* **8**(2), 1–13. https://doi.org/10.1523/ENEURO.0526-20.2021.

Breckenridge L and Almers W (1987) Currents through the fusion pore that forms during exocytosis of a secretory vesicle. *Nature* **328**(6133), 814–817.

Brewer KD *et al.* (2015) Dynamic binding mode of a Synaptotagmin-1–SNARE complex in solution. *Nature Structural & Molecular Biology* **22**(7), 555–564.

Brose N *et al.* (1995) Mammalian homologues of Caenorhabditis elegans unc-13 gene define novel family of C2-domain proteins. *The Journal of Biological Chemistry* **270**(42), 25273–25280. https://doi.org/10.1074/jbc.270.42.25273.

Brunger AT and Leitz J (2023) The Core complex of the Ca(2+)-triggered presynaptic fusion machinery. *Journal of Molecular Biology* **435**(1), 167853. https://doi.org/10.1016/j.jmb.2022.167853.

Bryant P *et al.* (2022) Improved prediction of protein-protein interactions using AlphaFold2. *Nature Communications* **13**(1). https://doi.org/10.1038/s41467-022-28865-w.

Butu IC, An D and O'Shaughnessy B (2025) How SNARE proteins generate force to fuse membranes. *Biophysical Journal* **124**(11), 1815–1827.

Bykhovskaia M (2015) Calcium binding promotes conformational flexibility of the neuronal Ca(2+) sensor synaptotagmin. *Biophysical Journal* **108**(10), 2507–2520. https://doi.org/10.1016/j.bpj.2015.04.007.

Bykhovskaia M (2021) SNARE complex alters the interactions of the Ca(2+) sensor synaptotagmin 1 with lipid bilayers. *Biophysical Journal* **120**(4), 642–661. https://doi.org/10.1016/j.bpj.2020.12.025.

Bykhovskaia M (2024) Dynamic formation of the protein-lipid prefusion complex. *Biophysical Journal* **123**(20), 3569–3586. https://doi.org/10.1016/j.bpj.2024.09.009.

Bykhovskaia M *et al.* (2013) Interaction of the complexin accessory helix with the C-terminus of the SNARE complex: Molecular-dynamics model of the fusion clamp. *Biophysical Journal* **105**(3), 679–690.

Cai HJ *et al.* (2008) Complexin II plays a positive role in Ca-triggered exocytosis by facilitating vesicle priming. *Proceedings of the National Academy of Sciences of the United States of America* **105**(49), 19538–19543. https://doi.org/10.1073/pnas.0810232105.

Callaway E (2024) Chemistry Nobel goes to developers of AlphaFold AI that predicts protein structures. *Nature* **634**(8034), 525–526. https://doi.org/10.1038/d41586-024-03214-7.

Chang C-W *et al.* (2016) Lipid-anchored synaptobrevin provides little or no support for exocytosis or liposome fusion. *Journal of Biological Chemistry* **291**(6), 2848–2857.

Chapman ER (2002) Synaptotagmin: A Ca2+ sensor that triggers exocytosis? *Nature Reviews Molecular Cell Biology* **3**(7), 498–508.

Chen YA *et al.* (2001) Sequential SNARE assembly underlies priming and triggering of exocytosis. *Neuron* **30**(1), 161–170. https://doi.org/10.1016/S0896-6273(01)00270-7.

Chen XC *et al.* (2002) Three-dimensional structure of the complexin/SNARE complex. *Neuron* **33**(3), 397–409. https://doi.org/10.1016/S0896-6273(02)00583-4.

Chernomordik LV and Kozlov MM (2008) Mechanics of membrane fusion. *Nature Structural & Molecular Biology* **15**(7), 675–683. https://doi.org/10.1038/nsmb.1455.

Cooke IR *et al.* (2005) Tunable generic model for fluid bilayer membranes. *Physical Review E* **72**(1). https://doi.org/10.1103/PhysRevE.72.011506.

Courtney KC, Wu LX, Mandal T, Swift M, Zhang Z, Alaghemandi M, Wu ZY, Bradberry MM, Deo C, Lavis LD, Volkmann N, Hanein D, Cui Q, Bao H and Chapman ER (2022) The complexin C-terminal amphipathic helix stabilizes the fusion pore open state by sculpting membranes. *Nature Structural & Molecular Biology* **29**(2), 97−+. https://doi.org/10.1038/s41594-021-00716-0.

Courtney KC *et al.* (2023) Synaptotagmin-7 outperforms synaptotagmin-1 to promote the formation of large, stable fusion pores via robust membrane penetration. *Nature Communications* **14**(1). https://doi.org/10.1038/s41467-023-42497-8.

Darre L *et al.* (2012) Mixing atomistic and coarse grain solvation models for MD simulations: Let WT4 handle the bulk. *Journal of Chemical Theory and Computation* **8**(10), 3880–3894. https://doi.org/10.1021/ct3001816.

Delacruz JB *et al.* (2021) Fusion pores with low conductance are cation selective. *Cell Reports* **36**(8), 109580. https://doi.org/10.1016/j.celrep.2021.109580.

DeLano WL (2002) Pymol: An open-source molecular graphics tool. *CCP4 Newsl. Protein Crystallogr* **40**(1), 82–92.

Deserno M (2009) Mesoscopic membrane physics: Concepts, simulations, and selected applications. *Macromolecular Rapid Communications* **30**(9–10), 752–771. https://doi.org/10.1002/marc.200900090.

Dhara M *et al.* (2016) V-SNARE transmembrane domains function as catalysts for vesicle fusion. *eLife* **5**. https://doi.org/10.7554/eLife.17571.

Diao J *et al.* (2012) A single vesicle-vesicle fusion assay for in vitro studies of SNAREs and accessory proteins. *Nature Protocols* **7**(5), 921–934.

Fang Q and Lindau M (2014) How could SNARE proteins open a fusion pore? *Physiology* **29**(4), 278–285.

Fasshauer D and Margittai M (2004) A transient N-terminal interaction of SNAP-25 and syntaxin nucleates SNARE assembly. *Journal of Biological Chemistry* **279**(9), 7613–7621. https://doi.org/10.1074/jbc.M312064200.

Fernandez I *et al.* (2001) Three-dimensional structure of the synaptotagmin 1 C2B-domain: Synaptotagmin 1 as a phospholipid binding machine. *Neuron* **32**(6), 1057–1069.

Fortoul N *et al.* (2015) Coarse-grained model of SNARE-mediated docking. *Biophysical Journal* **108**(9), 2258–2269. https://doi.org/10.1016/j.bpj.2015.03.053.

Fortoul N *et al.* (2018) Coarse-grained model for zippering of SNARE from partially assembled states. *The Journal of Physical Chemistry. B* **122**(48), 10834–10840. https://doi.org/10.1021/acs.jpcb.8b09502.

Gao Y *et al.* (2012) Single reconstituted neuronal SNARE complexes zipper in three distinct stages. *Science* **337**(6100), 1340–1343. https://doi.org/10.1126/science.1224492.

Ghahremanpour MM *et al.* (2010) Structural studies of SNARE complex and its interaction with complexin by molecular dynamics simulation. *Biopolymers: Original Research on Biomolecules* **93**(6), 560–570.

Ginsberg L (1978) Does Ca2+ cause fusion or lysis of unilamellar lipid vesicles? *Nature* **275**(5682), 758–760.

Gong L-W *et al.* (2007) Exocytotic catecholamine release is not associated with cation flux through channels in the vesicle membrane but Na+ influx through the fusion pore. *Nature Cell Biology* **9**(8), 915–922.

Han X *et al.* (2004) Transmembrane segments of syntaxin line the fusion pore of Ca2+−triggered exocytosis. *Science* **304**(5668), 289–292.

Han J *et al.* (2016) Synaptobrevin transmembrane domain determines the structure and dynamics of the SNARE motif and the linker region. *Biochimica et Biophysica Acta* **1858**(4), 855–865. https://doi.org/10.1016/j.bbamem.2016.01.030.

Harmalkar A *et al.* (2025) Reliable protein-protein docking with AlphaFold, Rosetta, and replica exchange. *eLife* **13**. https://doi.org/10.7554/eLife.94029.

Hartmann J and Lindau M (1995) A novel Ca2+−dependent step in exocytosis subsequent to vesicle fusion. *FEBS Letters* **363**(3), 217–220.

Hata Y *et al.* (1993) Synaptic vesicle fusion complex contains unc-18 homologue bound to syntaxin. *Nature* **366**(6453), 347–351. https://doi.org/10.1038/366347a0.

Hernandez JM *et al.* (2012) Membrane fusion intermediates via directional and full assembly of the SNARE complex. *Science* **336**(6088), 1581–1584.

Illya G and Deserno M (2008) Coarse-grained simulation studies of peptide-induced pore formation. *Biophysical Journal* **95**(9), 4163–4173. https://doi.org/10.1529/biophysj.108.131300.

Ingolfsson HI *et al.* (2017) Computational Lipidomics of the neuronal plasma membrane. *Biophysical Journal* **113**(10), 2271–2280. https://doi.org/10.1016/j.bpj.2017.10.017.

Jackson MB (2010) SNARE complex zipping as a driving force in the dilation of proteinaceous fusion pores. *Journal of Membrane Biology* **235**, 89–100.

Jaczynska K *et al.* (2023) Analysis of tripartite Synaptotagmin-1-SNARE-complexin-1 complexes in solution. *FEBS Open Bio* **13**(1), 26–50. https://doi.org/10.1002/2211-5463.13503.

Jaczynska K *et al.* (2025) A lever hypothesis for Synaptotagmin-1 action in neurotransmitter release. *Proceedings of the National Academy of Sciences* **122**(1), e2417941121.

Jahn R *et al.* (2024) Mechanisms of SNARE proteins in membrane fusion. *Nature Reviews. Molecular Cell Biology* **25**(2), 101–118. https://doi.org/10.1038/s41580-023-00668-x.

Jorquera RA *et al.* (2012) Complexin controls spontaneous and evoked neurotransmitter release by regulating the timing and properties of Synaptotagmin activity. *Journal of Neuroscience* **32**(50), 18234–18245. https://doi.org/10.1523/Jneurosci.3212-12.2012.

Jumper J *et al.* (2021) Highly accurate protein structure prediction with AlphaFold. *Nature* **596**(7873), 583–589. https://doi.org/10.1038/s41586-021-03819-2.

Jung JH (2019) Synaptic vesicles having large contact areas with the presynaptic membrane are preferentially Hemifused at active zones of frog neuromuscular junctions fixed during synaptic activity. *International Journal of Molecular Sciences* **20**(11). https://doi.org/10.3390/ijms20112692.

Kachar B *et al.* (1986) Morphological responses to calcium-induced interaction of phosphatidylserine-containing vesicles. *Biophysical Journal* **50**(5), 779–788.

Kemble GW *et al.* (1994) Lipid-anchored influenza hemagglutinin promotes hemifusion, not complete fusion. *Cell* **76**(2), 383–391.

Kesavan J *et al.* (2007) V-SNARE actions during Ca-triggered exocytosis. *Cell* **131**(2), 351–363. https://doi.org/10.1016/j.cell.2007.09.025.

Kim CS *et al.* (2002) Membrane topologies of neuronal SNARE folding intermediates. *Biochemistry* **41**(36), 10928–10933. https://doi.org/10.1021/bi026266v.

Knecht V and Grubmuller H (2003) Mechanical coupling via the membrane fusion SNARE protein syntaxin 1A: A molecular dynamics study. *Biophysical Journal* **84**(3), 1527–1547. https://doi.org/10.1016/S0006-3495(03)74965-0.

Kozlov MM *et al.* (2010) Protein-driven membrane stresses in fusion and fission. *Trends in Biochemical Sciences* **35**(12), 699–706.

Kümmel D *et al.* (2011) Complexin cross-links prefusion SNAREs into a zigzag array. *Nature Structural & Molecular Biology* **18**(8), 927–U1603. https://doi.org/10.1038/nsmb.2101.

Kundrotas PJ *et al.* (2012) Templates are available to model nearly all complexes of structurally characterized proteins. *Proceedings of the National Academy of Sciences of the United States of America* **109**(24), 9438–9441. https://doi.org/10.1073/pnas.1200678109.

Lakomek NA *et al.* (2019) Structural dynamics and transient lipid binding of synaptobrevin-2 tune SNARE assembly and membrane fusion. *Proceedings of the National Academy of Sciences of the United States of America* **116**(18), 8699–8708. https://doi.org/10.1073/pnas.1813194116.

Lázaro AS *et al.* (2024) The stability of the primed pool of synaptic vesicles and the clamping of spontaneous neurotransmitter release rely on the integrity of the C-terminal half of the SNARE domain of syntaxin-1A. *eLife* **12**, RP90775.

Li C *et al.* (1995) Ca2+-dependent and Ca2+-independent activities of neural and nonneural Synaptotagmins. *Nature* **375**(6532), 594–599. https://doi.org/10.1038/375594a0.

Li X *et al.* (2019) Symmetrical organization of proteins under docked synaptic vesicles. *FEBS Letters* **593**(2), 144–153. https://doi.org/10.1002/1873-3468.13316.

Li YZ *et al.* (2024) Complexin regulation of synaptic vesicle release: Mechanisms in the central nervous system and specialized retinal ribbon synapses. *Cell Communication and Signaling* **22**(1), Article number 581. https://doi.org/10.1186/s12964-024-01942-x.

Lindau M and Almers W (1995) Structure and function of fusion pores in exocytosis and ectoplasmic membrane fusion. *Current Opinion in Cell Biology* **7**(4), 509–517.

Lindau M *et al.* (2012) Coarse-grain simulations reveal movement of the synaptobrevin C-terminus in response to piconewton forces. *Biophysical Journal* **103**(5), 959–969. https://doi.org/10.1016/j.bpj.2012.08.007.

Liu HS *et al.* (2014) Synaptotagmin 7 functions as a Ca-sensor for synaptic vesicle replenishment. *eLife* **3**. https://doi.org/10.7554/eLife.01524.

Liu XX *et al.* (2016) Functional synergy between the Munc13 C-terminal C1 and C2 domains. *eLife* **5**. https://doi.org/10.7554/eLife.13696.

Ma C *et al.* (2013) Reconstitution of the vital functions of Munc18 and Munc13 in neurotransmitter release. *Science* **339**(6118), 421–425. https://doi.org/10.1126/science.1230473.

Ma L *et al.* (2015) Munc18-1-regulated stage-wise SNARE assembly underlying synaptic exocytosis. *eLife* **4**. https://doi.org/10.7554/eLife.09580.

Marrink SJ *et al.* (2004) Coarse grained model for semiquantitative lipid simulations. *Journal of Physical Chemistry B* **108**(2), 750–760. https://doi.org/10.1021/jp036508g.

Marrink SJ *et al.* (2007) The MARTINI force field: Coarse grained model for biomolecular simulations. *The Journal of Physical Chemistry. B* **111**(27), 7812–7824. https://doi.org/10.1021/jp071097f.

Martin JA *et al.* (2011) Complexin has opposite effects on two modes of synaptic vesicle fusion. *Current Biology* **21**(2), 97–105. https://doi.org/10.1016/j.cub.2010.12.014.

McDargh ZA *et al.* (2018) SNARE-mediated membrane fusion is a two-stage process driven by entropic forces. *FEBS Letters* **592**(21), 3504–3515. https://doi.org/10.1002/1873-3468.13277.

McMahon HT *et al.* (1995) Complexins: Cytosolic proteins that regulate Snap receptor function. *Cell* **83**(1), 111–119. https://doi.org/10.1016/0092-8674(95)90239-2.

McNew JA *et al.* (1999) The length of the flexible SNAREpin juxtamembrane region is a critical determinant of SNARE-dependent fusion. *Molecular Cell* **4**(3), 415–421. https://doi.org/10.1016/S1097-2765(00)80343-3.

Mehta N *et al.* (2024) The juxtamembrane linker of synaptotagmin 1 regulates Ca binding via liquid–liquid phase separation. *Nature Communications* **15**(1). https://doi.org/10.1038/s41467-023-44414-5.

Mirdita M *et al.* (2022) ColabFold: Making protein folding accessible to all. *Nature Methods* **19**(6), 679–682. https://doi.org/10.1038/s41592-022-01488-1.

Monticelli L *et al.* (2008) The MARTINI coarse-grained force field: Extension to proteins. *Journal of Chemical Theory and Computation* **4**(5), 819–834. https://doi.org/10.1021/ct700324x.

Mostafavi H *et al.* (2017) Entropic forces drive self-organization and membrane fusion by SNARE proteins. *Proceedings of the National Academy of Sciences of the United States of America* **114**(21), 5455–5460. https://doi.org/10.1073/pnas.1611506114.

Nikolaus J *et al.* (2010) Direct visualization of large and protein-free hemifusion diaphragms. *Biophysical Journal* **98**(7), 1192–1199.

Ohki S (1982) A mechanism of divalent ion-induced phosphatidylserine membrane fusion. *Biochimica et Biophysica Acta (BBA)-Biomembranes* **689**(1), 1–11.

Ohki S and Ohshima H (1985) Divalent cation-induced phosphatidic acid membrane fusion. Effect of ion binding and membrane surface tension. *Biochimica et Biophysica Acta (BBA)-Biomembranes* **812**(1), 147–154.

Oyler GA *et al.* (1989) The identification of a novel Synaptosomal-associated protein, Snap-25, differentially expressed by neuronal subpopulations. *Journal of Cell Biology* **109**(6), 3039–3052. https://doi.org/10.1083/jcb.109.6.3039.

Peitsch MC (1996) ProMod and Swiss-model: Internet-based tools for automated comparative protein modelling. *Biochemical Society Transactions* **24**, 274–279. https://doi.org/10.1042/bst0240274.

Perin MS *et al.* (1990) Phospholipid binding by a synaptic vesicle protein homologous to the regulatory region of protein kinase-C. *Nature* **345**(6272), 260–263. https://doi.org/10.1038/345260a0.

Radhakrishnan A *et al.* (2021) Symmetrical arrangement of proteins under release-ready vesicles in presynaptic terminals. *Proceedings of the National Academy of Sciences of the United States of America* **118**(5), e2024029118. https://doi.org/10.1073/pnas.2024029118.

Rand R *et al.* (1985) Dynamic morphology of calcium-induced interactions between phosphatidylserine vesicles. *Biophysical Journal* **47**(4), 483–489.

Risselada HJ and Grubmuller H (2012) How SNARE molecules mediate membrane fusion: Recent insights from molecular simulations. *Current Opinion in Structural Biology* **22**(2), 187–196. https://doi.org/10.1016/j.sbi.2012.01.007.

Risselada HJ *et al.* (2011) Caught in the act: Visualization of SNARE-mediated fusion events in molecular detail. *Chembiochem* **12**(7), 1049–1055. https://doi.org/10.1002/cbic.201100020.

Rizo J (2022) Molecular mechanisms underlying neurotransmitter release. *Annual Review of Biophysics* **51**(1), 377–408. https://doi.org/10.1146/annurev-biophys-111821-104732.

Rizo J, Jaczynska K and Rosenmund C (2025) Evaluation of synaptotagmin-1 action models by all-atom molecular dynamics simulations. *Febs Open Bio* **15**, 699–713. https://doi.org/10.1002/2211-5463.13966.

Rizo J *et al.* (2022) All-atom molecular dynamics simulations of Synaptotagmin-SNARE-complexin complexes bridging a vesicle and a flat lipid bilayer. *eLife* **11**. https://doi.org/10.7554/eLife.76356.

Rizo J *et al.* (2024) Molecular mechanism underlying SNARE-mediated membrane fusion enlightened by all-atom molecular dynamics simulations. *Proceedings of the National Academy of Sciences of the United States of America* **121**(16), e2321447121. https://doi.org/10.1073/pnas.2321447121.

Rohl CA *et al.* (2004) Modeling structurally variable regions in homologous proteins with rosetta. *Proteins: Structure, Function, and Bioinformatics* **55**(3), 656–677.

Rothman JE *et al.* (2023) Turbocharging synaptic transmission. *FEBS Letters* **597**(18), 2233–2249. https://doi.org/10.1002/1873-3468.14718.

Sabatini BL and Regehr WG (1996) Timing of neurotransmission at fast synapses in the mammalian brain. *Nature* **384**(6605), 170–172. https://doi.org/10.1038/384170a0.

Schiavo G *et al.* (1996) Calcium-dependent switching of the specificity of phosphoinositide binding to synaptotagmin. *Proceedings of the National Academy of Sciences* **93**(23), 13327–13332.

Sharma S and Lindau M (2017) T-SNARE Transmembrane domain clustering modulates lipid organization and membrane curvature. *Journal of the American Chemical Society* **139**(51), 18440–18443. https://doi.org/10.1021/jacs.7b10677.

Sharma S and Lindau M (2018) Molecular mechanism of fusion pore formation driven by the neuronal SNARE complex. *Proceedings of the National Academy of Sciences of the United States of America* **115**(50), 12751–12756. https://doi.org/10.1073/pnas.1816495115.

Sharma S *et al.* (2015) A coarse grained model for a lipid membrane with physiological composition and leaflet asymmetry. *PLoS One* **10**(12), e0144814. https://doi.org/10.1371/journal.pone.0144814.

Smirnova YG *et al.* (2019) Thermodynamically reversible paths of the first fusion intermediate reveal an important role for membrane anchors of fusion proteins. *Proceedings of the National Academy of Sciences of the United States of America* **116**(7), 2571–2576. https://doi.org/10.1073/pnas.1818200116.

Sollner T *et al.* (1993) SNAP receptors implicated in vesicle targeting and fusion. *Nature* **362**(6418), 318–324. https://doi.org/10.1038/362318a0.

Stein A *et al.* (2009) Helical extension of the neuronal SNARE complex into the membrane. *Nature* **460**(7254), 525–528. https://doi.org/10.1038/nature08156.

Südhof TC (2008) Neurotransmitter release. In Südhof TC and Starke K (eds.), Handbook of Experimental Pharmacology (HEP, volume **184**). *Pharmacology of Neurotransmitter Release*. Berlin, Heidelberg: Springer-Verlag, pp. 1–21.

Südhof TC (2013) Neurotransmitter release: The last millisecond in the life of a synaptic vesicle. *Neuron* **80**(3), 675–690. https://doi.org/10.1016/j.neuron.2013.10.022.

Südhof TC and Rothman JE (2009) Membrane fusion: Grappling with SNARE and SM proteins. *Science* **323**(5913), 474–477. https://doi.org/10.1126/science.1161748.

Toulmé E *et al.* (2024) Neurotransmitter release is triggered by a calcium-induced rearrangement in the Synaptotagmin-1/SNARE complex primary interface. *Proceedings of the National Academy of Sciences of the United States of America* **121**(42), e2409636121. https://doi.org/10.1073/pnas.2409636121.

Vardar G *et al.* (2022) Syntaxin-1A modulates vesicle fusion in mammalian neurons via juxtamembrane domain dependent palmitoylation of its transmembrane domain. *eLife* **11**, e78182. https://doi.org/10.7554/eLife.78182.

Vasin A *et al.* (2016) Interaction of the complexin accessory helix with synaptobrevin regulates spontaneous fusion. *Biophysical Journal* **111**(9), 1954–1964.

Veit M *et al.* (1996) Multiple palmitoylation of synaptotagmin and the t-SNARE SNAP-25. *FEBS Letters* **385**(1–2), 119–123. https://doi.org/10.1016/0014-5793(96)00362-6.

Vevea JD *et al.* (2021) Synaptotagmin 7 is targeted to the axonal plasma membrane through γ-secretase processing to promote synaptic vesicle docking in mouse hippocampal neurons. *eLife* **10**, e67261. https://doi.org/10.7554/eLife.67261.

Voleti R *et al.* (2020) Ca2+−dependent release of synaptotagmin-1 from the SNARE complex on phosphatidylinositol 4, 5-bisphosphate-containing membranes. *eLife* **9**, e57154.

Warner JM and O'Shaughnessy B (2012a) Evolution of the hemifused intermediate on the pathway to membrane fusion. *Biophysical Journal* **103**(4), 689–701.

Warner JM and O'Shaughnessy B (2012b) The hemifused state on the pathway to membrane fusion. *Physical Review Letters* **108**(17), 178101.

Warner JM *et al.* (2023) A hemifused complex is the hub in a network of pathways to membrane fusion. *Biophysical Journal* **122**(2), 374–385. https://doi.org/10.1016/j.bpj.2022.12.003.

Waterhouse A *et al.* (2018) SWISS-MODEL: Homology modelling of protein structures and complexes. *Nucleic Acids Research* **46**(W1), W296–W303. https://doi.org/10.1093/nar/gky427.

Weber T *et al.* (1998) SNAREpins: Minimal machinery for membrane fusion. *Cell* **92**(6), 759–772.

White KI *et al.* (2018) Structural principles of SNARE complex recognition by the AAA plus protein NSF. *eLife* **7**, e38888. https://doi.org/10.7554/eLife.38888.

Wiederhold K and Fasshauer D (2009) Is assembly of the SNARE complex enough to fuel membrane fusion? *Journal of Biological Chemistry* **284**(19), 13143–13152.

Witkowska A *et al.* (2021) Tight docking of membranes before fusion represents a metastable state with unique properties. *Nature Communications* **12**(1), 3606. https://doi.org/10.1038/s41467-021-23722-8.

Wu ZY *et al.* (2024) Synaptotagmin 7 docks synaptic vesicles to support facilitation and Doc2α-triggered asynchronous release. *eLife* **12**. https://doi.org/10.7554/eLife.90632.

Yadav D *et al.* (2024) A look beyond the QR code of SNARE proteins. *Protein Science* **33**(9), e5158. https://doi.org/10.1002/pro.5158.

Zhang YL and Hughson FM (2021) Chaperoning SNARE folding and assembly. *Annual Review of Biochemistry* **90**, 581–603. https://doi.org/10.1146/annurev-biochem-081820-103615.

Zhang QC *et al.* (2010) Protein interface conservation across structure space. *Proceedings of the National Academy of Sciences of the United States of America* **107**(24), 10896–10901. https://doi.org/10.1073/pnas.1005894107.

Zhao W-D *et al.* (2016) Hemi-fused structure mediates and controls fusion and fission in live cells. *Nature* **534**(7608), 548–552.

Zheng W (2014) All-atom and coarse-grained simulations of the forced unfolding pathways of the SNARE complex. *Proteins* **82**(7), 1376–1386. https://doi.org/10.1002/prot.24505.

Zhou QJ, **Lai Y**, **Bacaj T**, **Zhao ML**, **Lyubimov AY**, **Uervirojnangkoorn M**, **Zeldin OB**, **Brewster AS**, **Sauter NK**, **Cohen AE**, **Soltis SM**, **Alonso-Mori R**, **Chollet M**, **Lemke HT**, **Pfuetzner RA**, **Choi UB**, **Weis WI**, **Diao JJ**, **Südhof TC and Brunger AT** (2015) Architecture of the synaptotagmin-SNARE machinery for neuronal exocytosis. *Nature* **525**(7567), 62−+. https://doi.org/10.1038/nature14975.

Zhou Q *et al.* (2017) The primed SNARE–complexin–synaptotagmin complex for neuronal exocytosis. *Nature* **548**(7668), 420–425.

Zimmerberg J *et al.* (1993) Mechanisms of membrane fusion. *Annual Review of Biophysics and Biomolecular Structure* **22**(1), 433–466.